

**EUROPEAN ORGANIZATION FOR NUCLEAR RESEARCH  
ORGANISATION EUROPEENNE POUR LA RECHERCHE NUCLEAIRE**

**CERN - PS DIVISION**

PS/ RF/ Note 97-14

**RF MEASUREMENTS ON ACCELERATING  
STRUCTURE HCS1**

R. Bossart and M. Chanudet

Geneva, Switzerland  
9 September 1997

# RF MEASUREMENTS ON ACCELERATING STRUCTURE HCS1

R. Bossart and M. Chanudet

## 1. Introduction

The tuning of the accelerating structure HCS1 was finished at LAL Orsay on August 1, 1997. The structure was transported to CERN and the RF measurements were resumed at CERN on August 12, 1997. Three types of measurements were carried out :

1. Pulse response of reflected and transmitted power for an RF pulse with a pulse duration of 0.8 - 4.5  $\mu$ s, measured by the automatic calibrated peak power-meter GMC 478 A.
2. CW measurements with the network analyser HP 8753 B providing the transmission parameter S21 between input and output coupler and the reflection parameter S11 at the input and output coupler.
3. Perturbation measurements with a ceramic bead  $\varnothing$  1 mm pulled by a nylon wire along the centre axis through the structure, providing information about the relative field strength and the phase advance between the cells and input/output couplers.

## 2. Pulse Response of HCS1

The pulse response of a TW structure is limited by the frequency bandwidth of the passband. For operation at  $11\pi/12$  mode, an important amount of the pulse spectrum is outside the upper end of the passband ending with the  $\pi$ -mode. The group velocity of the travelling wave decreases towards the  $\pi$ -mode and the filling time of the structure increases accordingly. The input power outside the bandwidth of the coupler is reflected back to the source at the beginning and end of the RF pulse , as known from SW structures.

In order to quantify the amount of pulse power reflected, an RF pulse of 1.5  $\mu$ s duration was applied to the HCS1 input. At the nominal frequency close to the  $\pi$ -mode, the instantaneous power reflected at the input coupler amounts to 27% for a pulse rise time of 100 ns. The reflected power decays quasi-exponentially with an e-folding time of  $\tau/2 \cong 120$  ns (see fig. 1). The frequency bandwidth of the input coupler is given by  $f = 1/\pi\tau \cong 1300$  kHz.

Since the bandwidth of the klystron driving the HCS section is about 10 MHz, the rise/fall time of the RF pulse is as short as 80 - 100 ns. A longer rise/fall time of 500 ns at the HCS input is required to reduce the reflected peak power to 7% of the incident power (see fig. 2).

The power reflected back to the klystron can endanger the RF windows of the klystron and eventually cause RF breakdown. Since the reflection is as short as  $\tau = 120$  ns, the energy of the reflection is  $W = P\tau$ . This energy is definitely smaller than for a continuous reflection of 1.5 MW lasting 4.5  $\mu$ s, specified as maximum reflection for safe klystron operation. Power tests with klystron MDK 29 are planned to check if the klystron withstands a reflected power of 7% or 4 MW during 120 ns.

It will not be easy to slow down the rise time of the klystron output pulse to 500 ns, as the klystron is working at saturation. A rise time of 500 ns is equivalent to a frequency bandwidth of about 2 MHz. It must be checked by power tests if a cavity filter 400 W with a bandwidth of 2 MHz at the klystron input will provide the necessary increase of the pulse rise/fall time at the HCS input.

The fill time of the HCS1 structure has been measured between input and output coupler (see fig. 3). The pulse width has been increased to 2.5  $\mu$ s, so that one can clearly distinguish between the transient rise time lasting for about 1.5  $\mu$ s and the steady state excitation of the accelerating field in the output coupler. The waveforms of the transmitted and reflected power clearly show that there are multiple internal reflections of the travelling wave inside the HCS section. Because of the limited bandwidth of the HCS section, the rise time of the accelerating field is slowed down to about 1 - 1.5  $\mu$ s. The pulse response at the output coupler is much slower than at the input coupler because of the phase dispersion between the upper and lower half of the frequency spectrum of the RF pulse. Furthermore, the internal mismatches between cells and couplers cause additional retardation. In conclusion, the slow fill time of the HCS structures is a direct consequence of the small frequency separation between the modes  $11\pi/12$  and  $\pi$ .

In the original design of HCS a fill time of 0.7  $\mu$ s was assumed. It was foreseen that a rectangular RF pulse of 120 MW power and 0.8  $\mu$ s duration would provide an accelerating gradient of 60 MeV/m. Because of the longer fill time of the HCS section, the RF pulse duration must be increased from 0.8  $\mu$ s to 1.5  $\mu$ s. Therefore the RF pulse power delivered by the LIPS pulse compression system will be reduced to 60 MW for a quasi-rectangular RF pulse. The accelerating gradient of the beam will be reduced to 70% of the design value. Originally, the HCS sections had been designed for a beam loading of 1  $\mu$ C. A smaller accelerating gradient of 70% of the nominal value will reduce the maximum beam intensity to 700 nC for the same relative beam loading as in the original design of HCS<sup>1)</sup>.

### 3. CW Measurements with Network Analyser

By means of the network analyser, the transmission parameter S21 was measured between the input and output coupler of HCS1, revealing the attenuation factor and the group delay of the TW structure.

The acceleration mode  $11\pi/12$  is separated only by 450 kHz from the  $\pi$ -mode at the end of the TW passband (see fig. 4). The TW passband spreads from O-mode to  $\pi$ -mode over a frequency bandwidth of 23.4 MHz. The attenuation factor from the input to the output coupler of the TW structure is -4.3 dB at the nominal acceleration frequency  $f_0 = 3005.25$  MHz (marker 1) for air at 28°C. The neighbour mode  $5\pi/6$  is found at 3040.0 MHz (marker 2). It should be noticed that there is a strong standing wave SW pattern comprising 13 resonance peaks over the TW passband. The 13 resonance peaks correspond to the SW modes of the 13 acceleration cells and 2 coupler cells. The  $\pi$ -mode does not appear as a distinct resonance peak. The SW pattern indicates that there is an important impedance mismatch among acceleration cells and couplers.

The phase information of the S21 measurement is presented in figure 5 in the form of the group delay between input to output coupler. Because of the internal mismatches between cells and due to the limited bandwidth of the HCS1 structure, the delay measurement  $T_d = d\phi/d\omega$  does not truly represent the fill time of the structure. The maximum delay of 910 ns measured at 450 kHz above the nominal frequency  $f_0$  corresponds to the  $\pi$ -mode. As a matter of fact, the RF pulse at the  $\pi$ -mode frequency 3005.87 MHz propagates as fast as the mode  $11\pi/12$  in HCS1 (see fig. 1). The propagation and rise time of the  $\pi$ -mode at the output coupler can be explained by RF losses in the cells and by frequency deviations among cells.

### 4. Perturbation Measurements with Test Bead

The perturbation method established by Slater allows to measure the relative field strength and the phase advance between the cells of an accelerating structure.

The perturbation measurements were performed with a ceramic bead of diameter  $\varnothing$  1mm  $\times$  13 mm length, pulled along the centre axis of the accelerator structure by a nylon wire  $\varnothing$  0.4 mm. The nylon wire reduces the resonance frequency of HCS1 by -175 kHz.

If the test bead is introduced into the accelerator cavity, it causes a frequency drop and an impedance mismatch of the cell where the bead is. A fraction of the incident wave is reflected by the impedance mismatch backwards towards the input coupler and is measured by the network analyser.

Care must be taken that only the reflection from the test bead is measured and not the multiple reflections caused by slight mismatches between the cells and the couplers. The unavoidable reflections of the travelling wave caused by cell mismatches, which are very important at a frequency close to the  $\pi$ -mode, were

removed from the measurement S11 by calibrating the network analyser with the unperturbed HCS1 structure as load standard. The test bead  $\varnothing 1 \times 13$  mm causes a local power reflection of -10 dB of the incident wave. Both the incident and the reflected wave are attenuated along the TW structure by  $-0.3$  dB/cell. The amplitude range of the perturbation measurement is very large, since the reflection reference level of the unperturbed HCS1 structure can be reduced to -60 dB by the calibration technique of the network analyser with the unperturbed structure. As the amplitude range of the perturbation method is enlarged, a smaller test bead can be used to reduce the cell perturbation.

The perturbation measurement with a ceramic bead provides both amplitude and phase information of the cells probed. The test bead is pulled in 20 seconds through the structure and the network analyser, set to a fixed frequency and a receiver bandwidth of 30 Hz, records the reflected signal S11 during a sweep time of 20 seconds. The perturbation measurement is easy and quick and provides a wealth of information about all cells and couplers.

The amplitude of the reflection in each cell reveals the relative electric field strength  $(E_z/E_0)^2$  at the place  $z$  of the test bead (see fig. 7). The measurement of S11 shows that the field strength at the input and output couplers is 2 dB higher than the average field in the cells. Among the cells there is an amplitude modulation of  $\pm 1.5$  dB.

The phase plot in figure 8 indicates the relative phase of the reflection S11 measured at the input of the hybrid waveguide junction (see fig. 5). The phase advance, as measured by S11 from cell to cell, represents twice the phase advance  $\delta$  seen by the beam. Since the phase  $\delta$  per cell is close to  $\pi$  for HCS1, the network analyser displays the phase measurement of  $\varphi$  modulo  $2\pi$  :  $\varphi = 2\pi - 2\delta$ . For the acceleration mode  $\delta = 11\pi/12$  of HCS1, the phase advance  $\varphi$  of S11 was adjusted at LAL Orsay by a mechanical deformation of the thin cell walls for  $\varphi = 30^\circ$  per cell. The signal S11 was reflected by a metal piston in the HCS1 structure, a method which is delicate for a large iris aperture and for an acceleration frequency close to the  $\pi$ -mode.

In figure 7, three groups of cells can be distinguished. From the input coupler to cell #5, the average phase advance per cell is  $\varphi = 46^\circ$ . From cell #5 to cell #10 :  $\langle \varphi \rangle = 26^\circ$ ; in the last three cells #11 - 13 :  $\langle \varphi \rangle = 68^\circ$ .

Measured from input to output coupler, the average phase advance  $\delta$  seen by the beam amounts to  $\delta = 159^\circ$  instead of  $165^\circ$ . The phase error between input and output coupler amounts to  $14 \times 6^\circ = 84^\circ$  for beam acceleration. Such a large phase error means that the last cells do not contribute enough to the beam acceleration. It is therefore mandatory to correct the large errors of cells #11-13, hopefully by pulling outwards on the thin wall areas foreseen for mechanical deformation of the cells. New tuning screws for HCS are being developed by J.C. Godot and A. Ruck. It is hoped that the phase advance  $\delta$  and the field strength  $E_z$  can be equalized among all cells by means of these new tuning screws.

The test bead does not affect the coupling of the probed cell with the neighbour cells as heavily as the detuning method does by a metal piston in the downstream cell. Due to the large iris diameter, the cells are coupled strongly to each other even if the downstream cell is detuned by a metal piston of the same diameter as the iris aperture. During the tuning procedure of HCS1 with a metal piston it was observed that the phase delay measured between two cells changed when the next cell downstream was deformed. This means that the metal piston does not completely decouple from the downstream cell.

## **5. Power Tests of HCS1**

In the design study of HCS1, an input power of 120 MW during 0.8  $\mu\text{s}$  was foreseen in order to accelerate the beam by a maximum field strength  $E_z = 60 \text{ MV/m}$  on the crest of the travelling wave. The electric field strength on the irises between the cells is twice as high and will cause strong field emission at 120 MV/m and probably breakdown of the RF field in the HCS structure. In order to explore the RF breakdown limits of HCS1, it is planned to conduct RF power tests with LIPS pulse compression of the klystron pulse. It is expected that the LIPS pulse compression scheme with double phase ramping is able to produce a quasi-rectangular power pulse of 60 MW during 1.5  $\mu\text{s}$  at the LIPS output or 120 MW during 0.8  $\mu\text{s}$ . However, in order to protect the klystron against transient reflections from the HCS1 structure, the rise and fall time of the power pulse must be stretched to 0.5  $\mu\text{s}$ . The longer rise/fall time of the LIPS pulse compression will reduce the peak power gain factor proportionally to the length of the output pulse.

A short RF pulse will always cause an important transient power reflection by any travelling wave section designed for slow group velocity and high acceleration gradient. It is therefore important to test the breakdown limits of the HCS1 section powered by an old 30 MW klystron with LIPS.

## **6. Reference**

- 1) G. Bienvenu and J. Gao, A high current, high gradient electron double accelerating structure, Proc. European Part. Acc. Conf. Barcelona, 1996, p. 495.

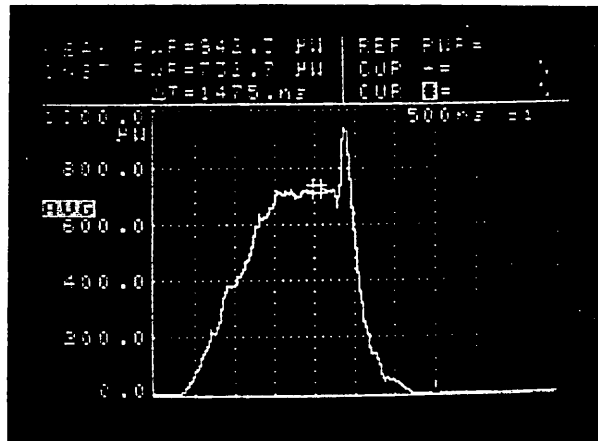
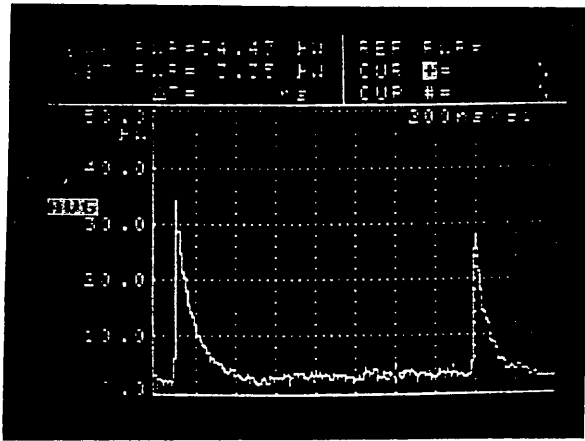
Figure 1

Reflected and transmitted RF power of HCS1 versus pulse time

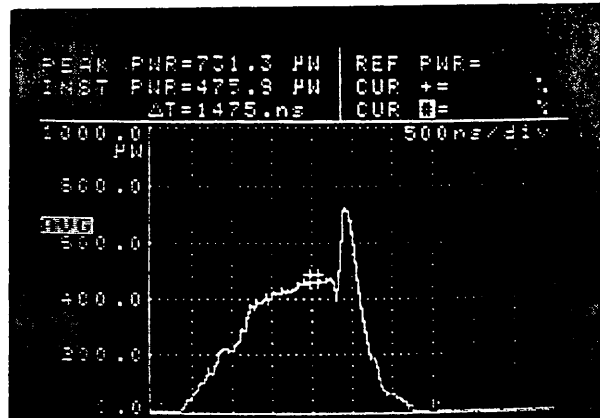
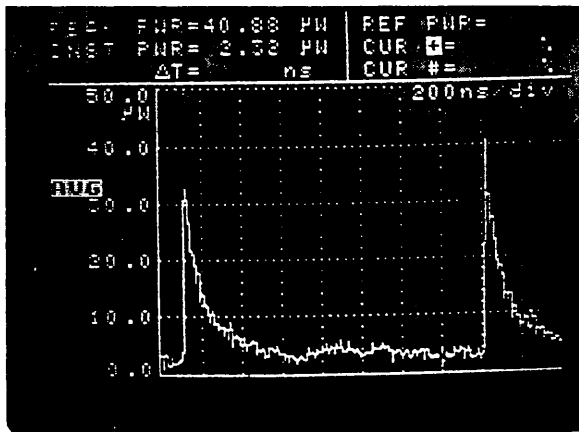
Input Power :  $P = 3.5 \text{ mW}$  , Pulse Width :  $PW = 2 \mu\text{s}$  , Rise / Fall Time :  $t_r = 10 \text{ ns}$   
 Reflection Coupler :  $a = -19 \text{ dB} = 0.013$  ,  $T = 27.4 \text{ deg}$  ,  $H = 68 \%$

Reflected Power

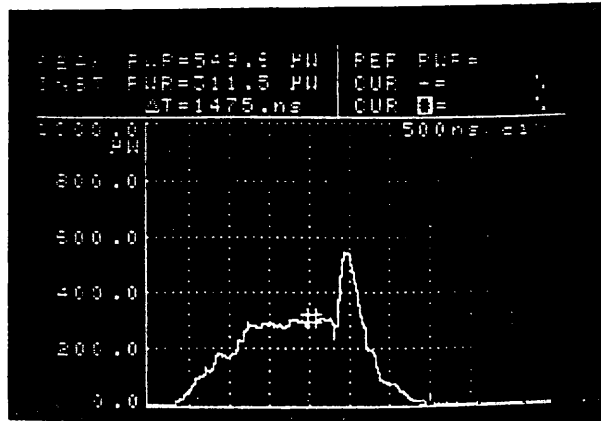
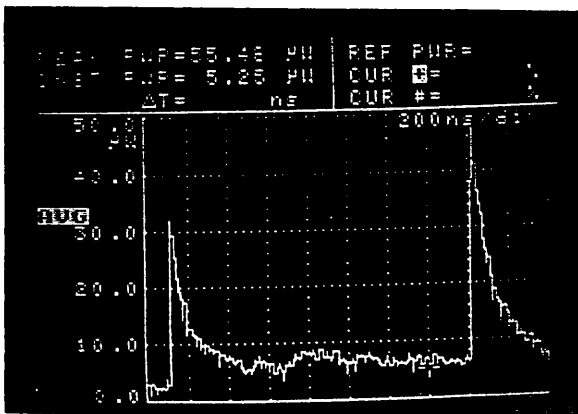
Transmitted Power



$r^2 = 70\%$        $f_0 = 3005.420 \text{ MHz}$  ,  $t_g = 660 \text{ ns}$  ,       $t^2 = 40\%$



$r^2 = 80\%$        $f_0 + 0.3 \text{ MHz} = 3005.720 \text{ MHz}$  ,  $t_g = 820 \text{ ns}$  ,       $t^2 = 27\%$



$r^2 = 110\%$        $f_0 + 0.4 \text{ MHz} = 3005.870 \text{ MHz}$  ,  $t_g = 910 \text{ ns}$  ,       $t^2 = 18\%$   
 $r^2 = 10\% \text{ CW}$

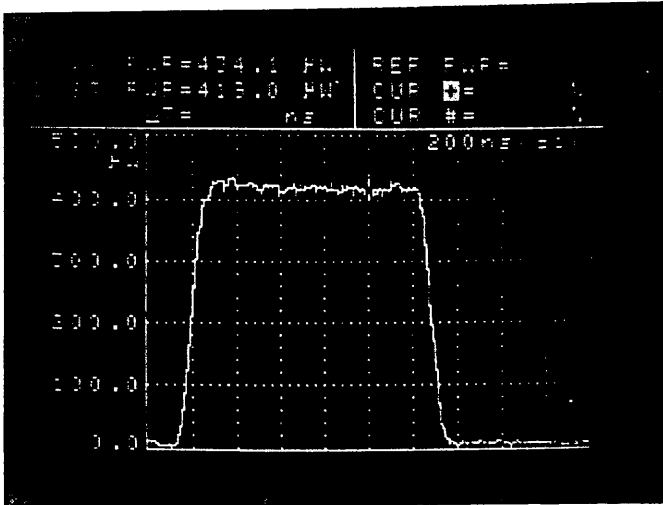
Figure 2

Reflected RF power of HCS1 versus pulse rise/fall time

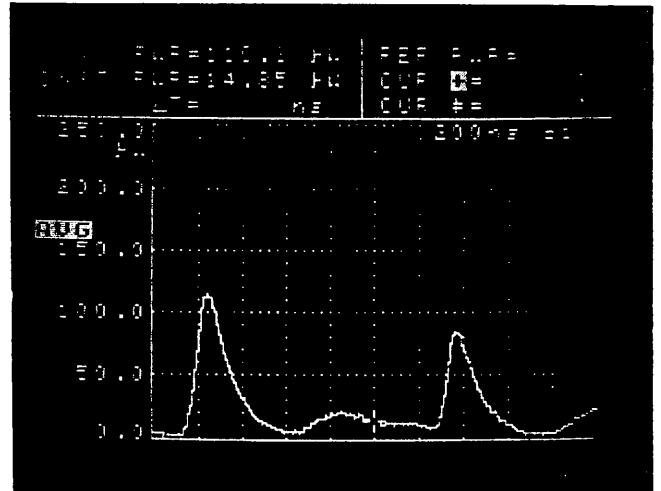
Frequency : 3005.5 MHz (nominal)

Incident Power

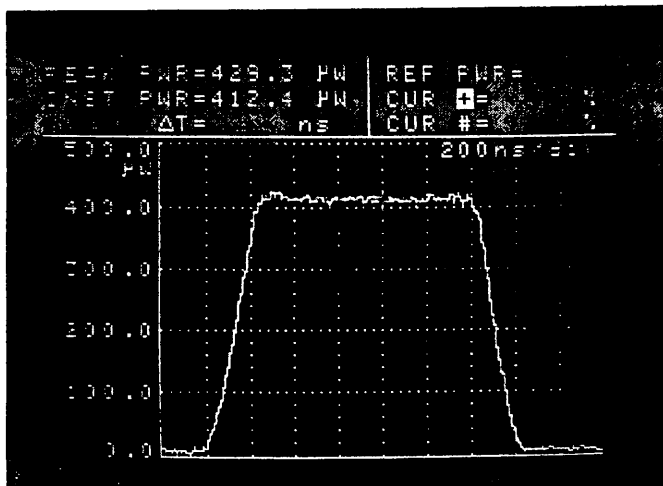
Reflected Power



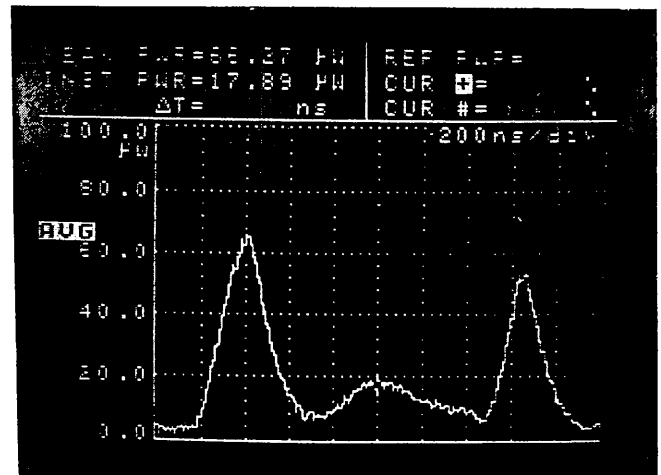
Rise Time  $t_r = t_f = 0.1 \mu s$



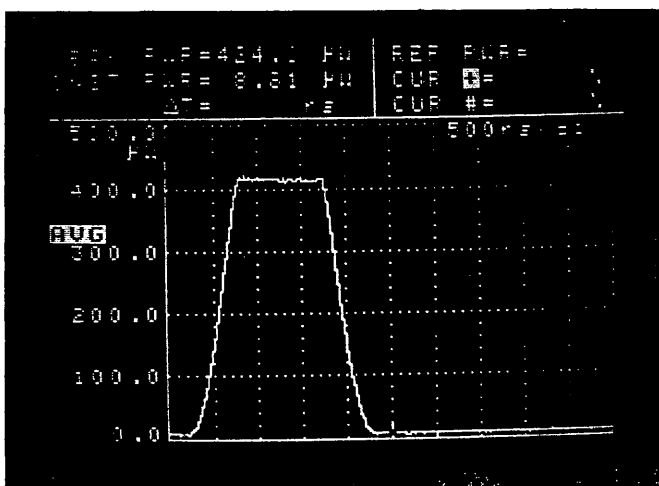
Reflection  $r^2 = 27\%$  peak



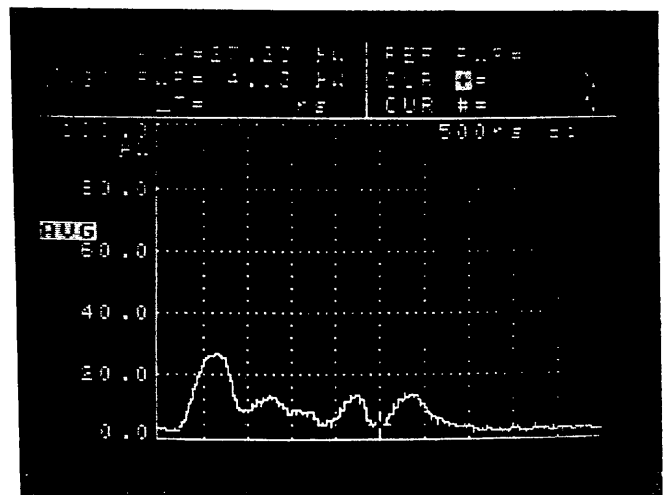
Rise Time  $t_r = t_f = 0.2 \mu s$



Reflection  $r^2 = 16\%$  peak



Rise Time  $t_r = t_f = 0.5 \mu s$



Reflection  $r^2 = 7\%$  peak



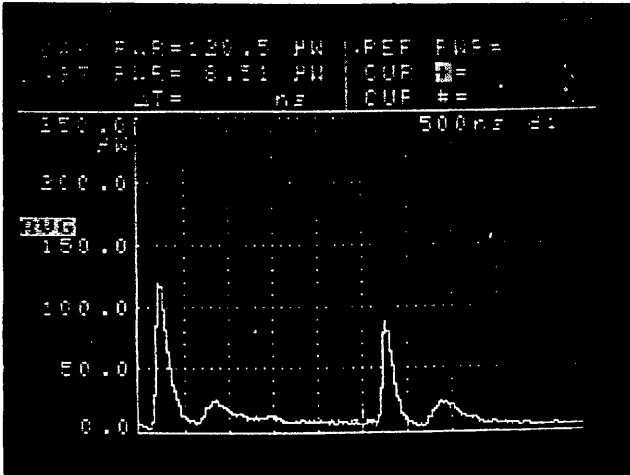
Figure 3

Reflected and transmitted RF power of HCS1 versus frequency mode

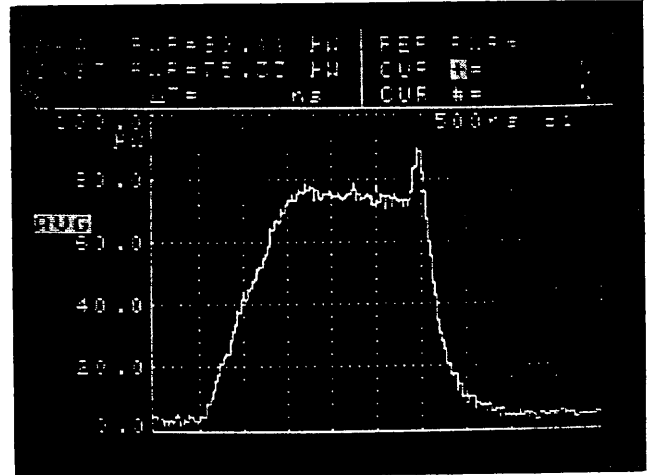
Input Power :  $P = 40 \text{ mW}$ , Pulse Width :  $PW = 2.5 \mu\text{s}$ , Rise Time :  $t_r = 100 \text{ ns}$   
 Measurement Coupler :  $a = -19 \text{ dB}$ ,  $T = 26.3 \text{ deg}$ ,  $H = 68\%$

Reflected Power

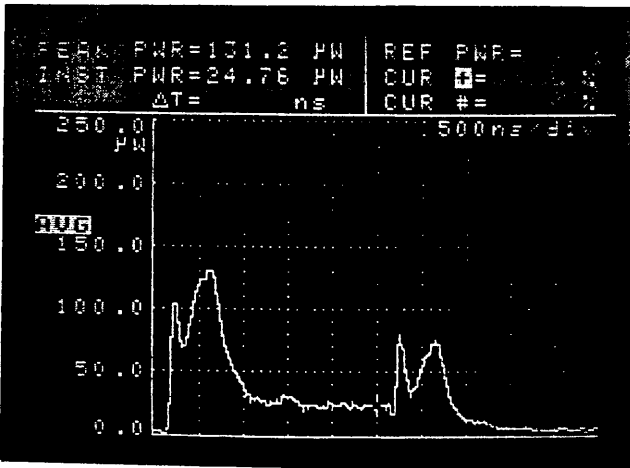
Transmitted Power



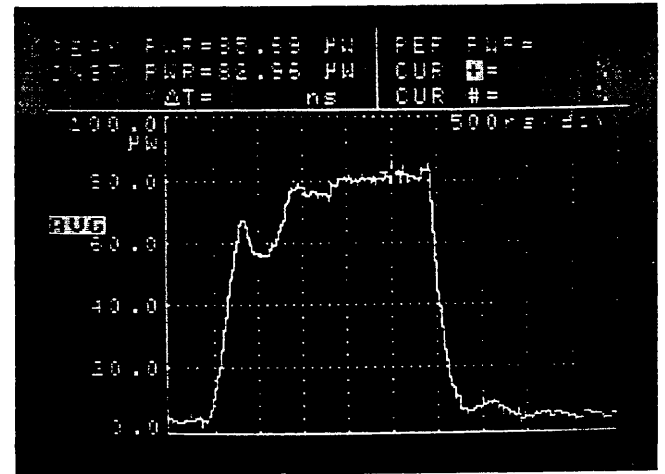
Mode  $11\pi/12$  :  $f_0 = 3005.5 \text{ MHz}$ ,  $r^2 = 30\% \text{ pk}$   
 $r_0^2 = 2\% \text{ CW}$



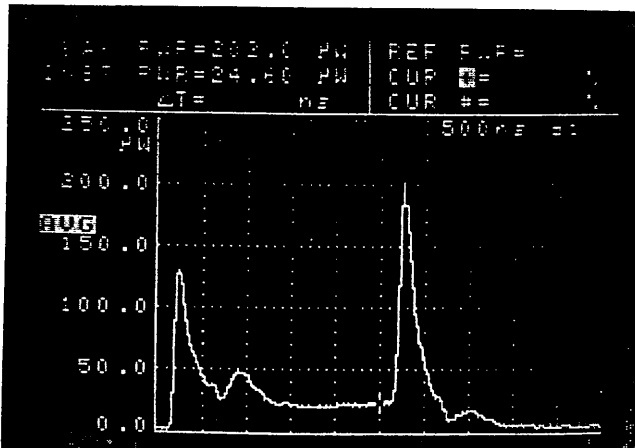
$t^2 = 19\%$ ,  $T_d = 660 \text{ ns}$



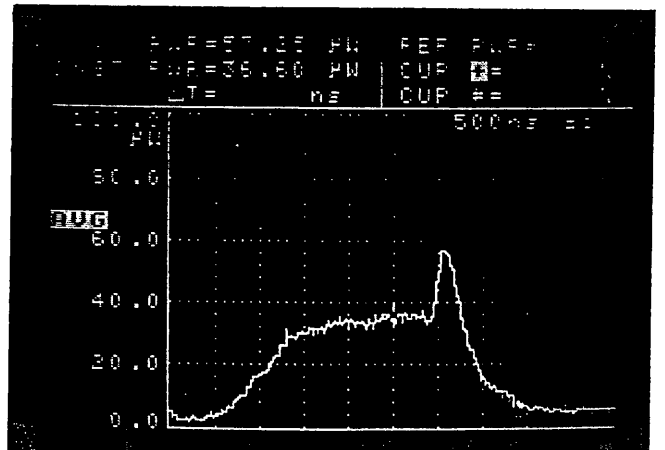
Mode  $5\pi/6$  :  $f_0 - 1.4 \text{ MHz}$ ,  $r^2 = 33\% \text{ pk}$   
 $r_0^2 = 6\% \text{ CW}$



$t^2 = 21\%$ ,  $T_d = 550 \text{ ns}$



Mode  $\pi$  :  $f_0 + 0.45 \text{ MHz}$ ,  $r^2 = 50\% \text{ pk}$   
 $r_0^2 = 6\% \text{ CW}$



$t^2 = 9\%$ ,  $T_d = 910 \text{ ns}$

CH1 S21 109 MAG 10 dB/ REF -25 dB Δ: -7.3112 dB  
 3 005.250 600 MHZ

Cor MARKER 1  
 3.0052506 GHz

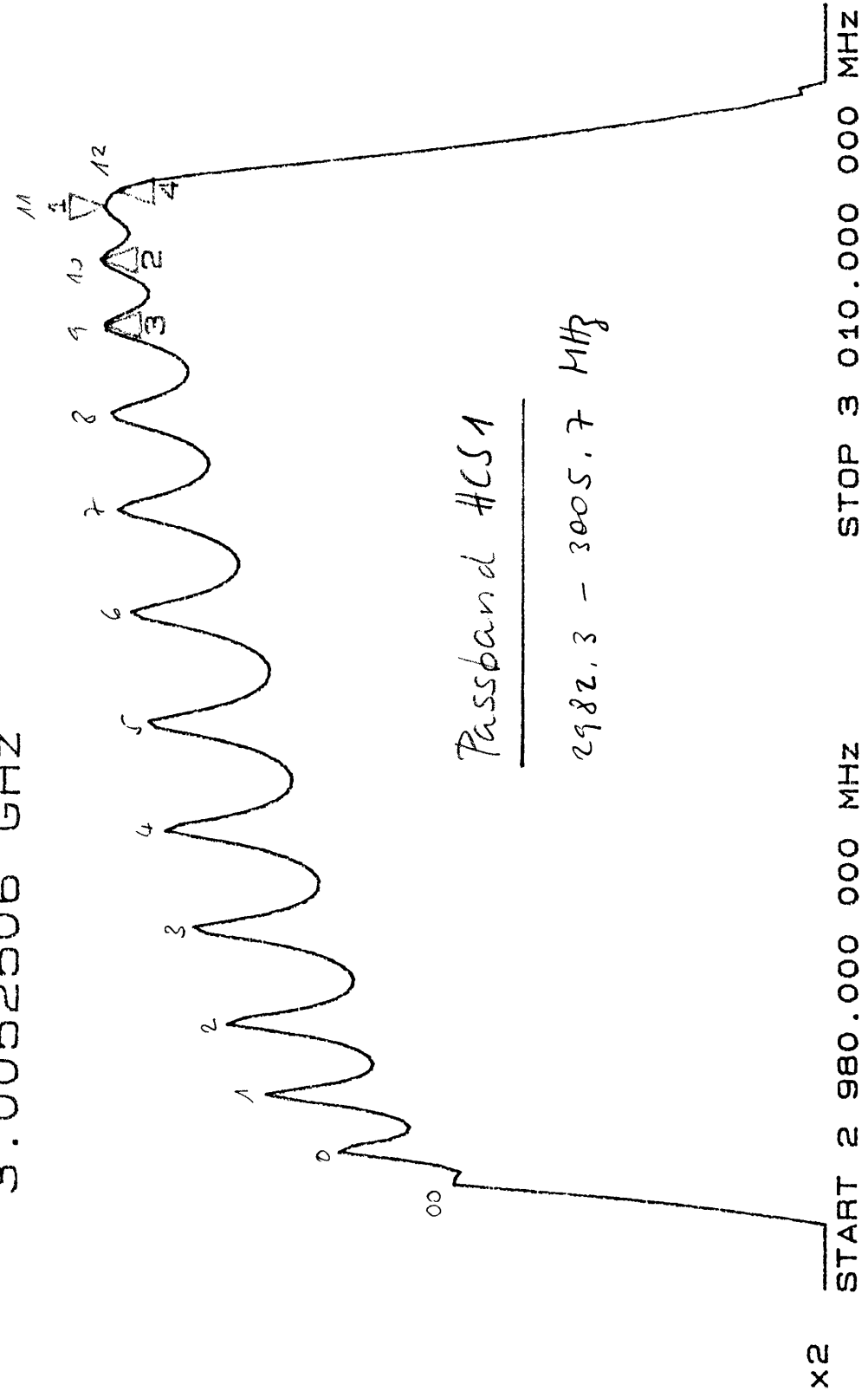
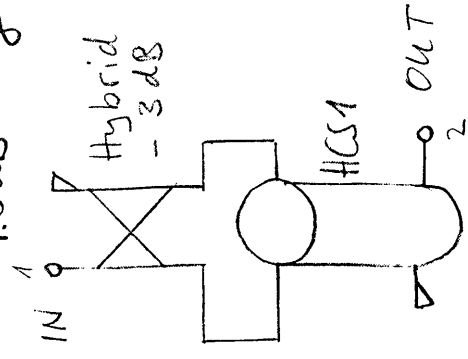


Figure 4

Attenuation In/Out

- 1: 3005.250 MHz  
-4.3 dB
- 2: 3004.010 MHz  
-3.7 dB
- 3: 3002.445 MHz  
-3.9 dB
- 4: 3005.660 MHz  
-7.0 dB



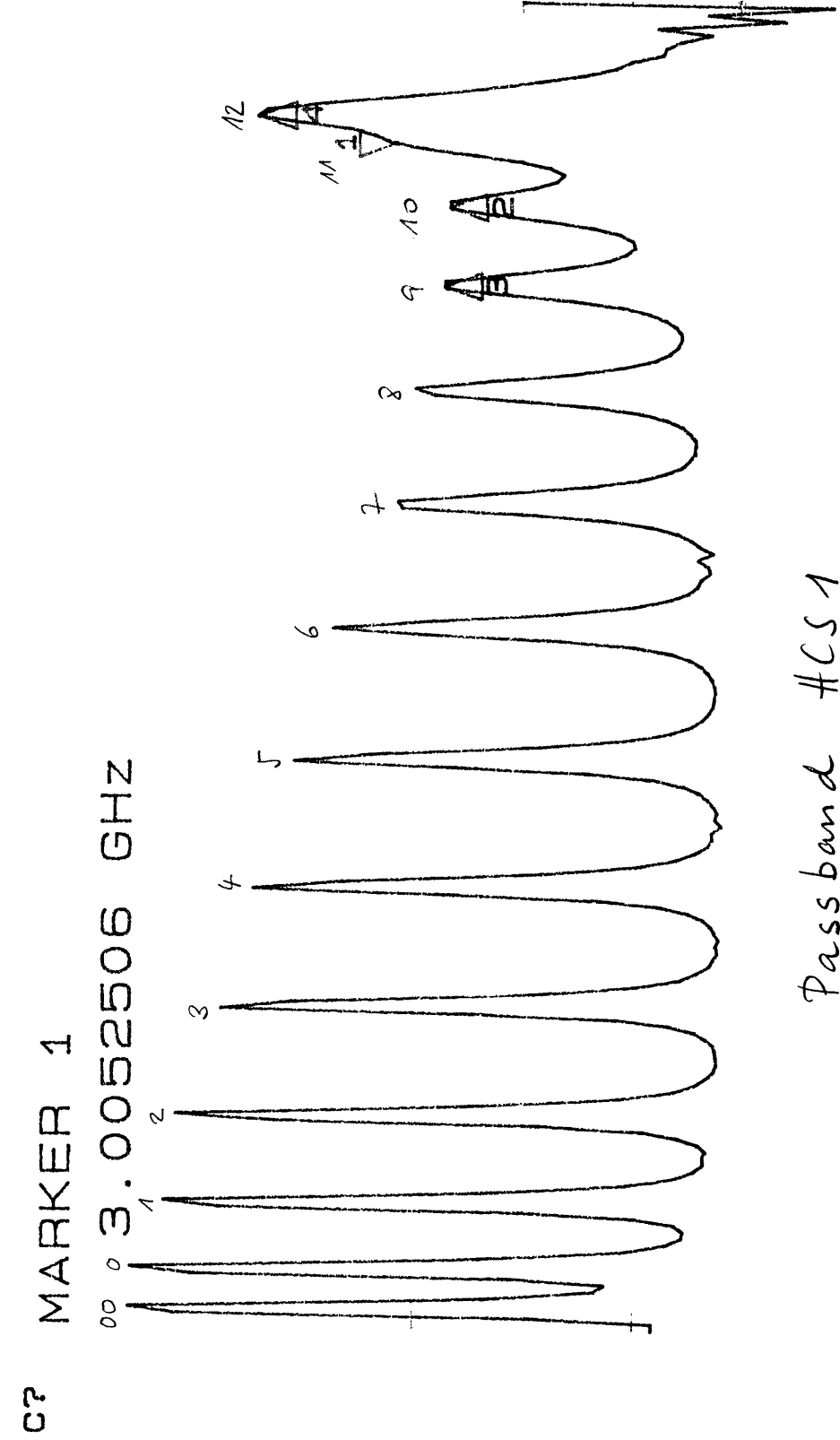
T = 28.0 °C

13.8.97

CH1 S21 delay 200 ns / REF 600 ns 1: 630.91 ns  
 3 005.250 600 MHz

Figure 5

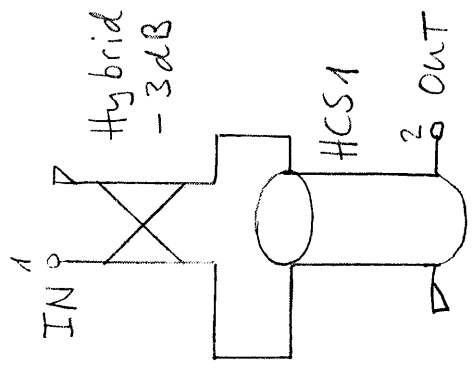
Group Delay



1: 3005.250 MHz  
 $T_g = 630 \text{ ns}$

2: 3004.010 MHz  
 $T_g = 550 \text{ ns}$

3: 3002.445 MHz  
 $T_g = 570 \text{ ns}$



Passband #CS1  
 Modes 00 - 12

$T = 28.0^\circ \text{C}$

x2 START 2 982.000 000 MHz STOP 3 008.000 000 MHz

13.8.97

CH1 S<sub>11</sub> 1 U FS

4: 17.687 mU -53.579 °

Ⓜ

3 005.690 618 MHz

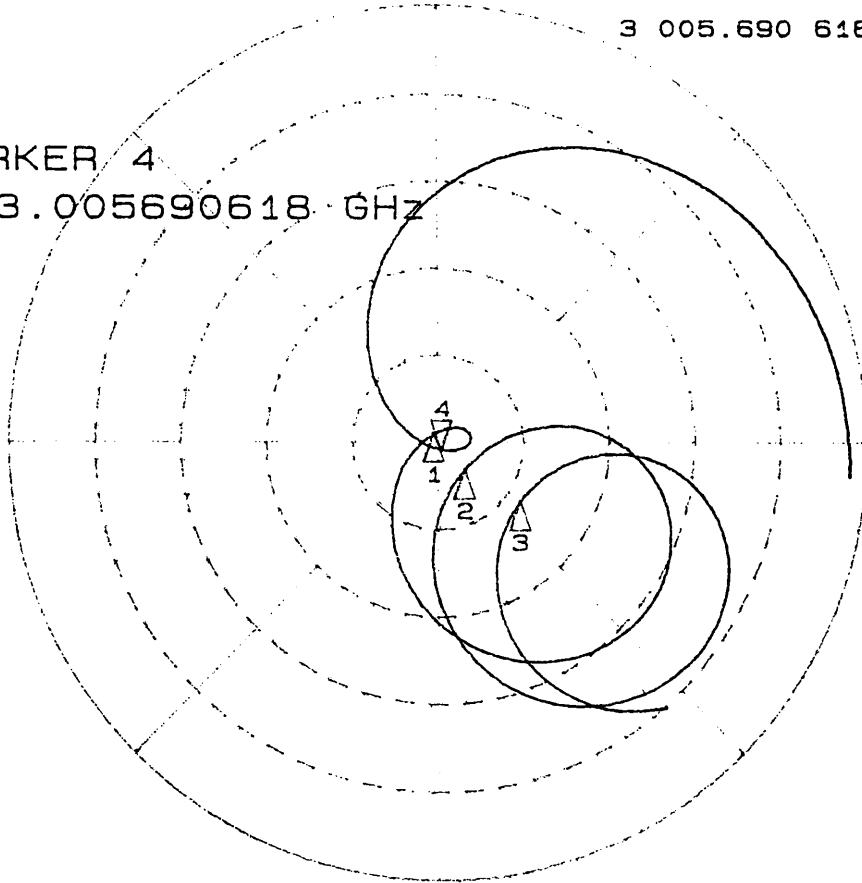
Figure 6

C? PK

MARKER 4

3.005690618 GHz

Reflection of HCS1  
at Input Coupler



4: 3005.690 MHz  
S<sub>11</sub> = -35 dB

1: 3004.420 MHz  
S<sub>11</sub> = -32 dB

2: 3004.095 MHz  
S<sub>11</sub> = -21 dB

T = 26.2 °C

14.8.97

x2

START 3 002.000 000 MHz

STOP 3 008.000 000 MHz

CH1 S<sub>11</sub> 1 U FS

2: 421.39 mU -111.24 °

Ⓜ

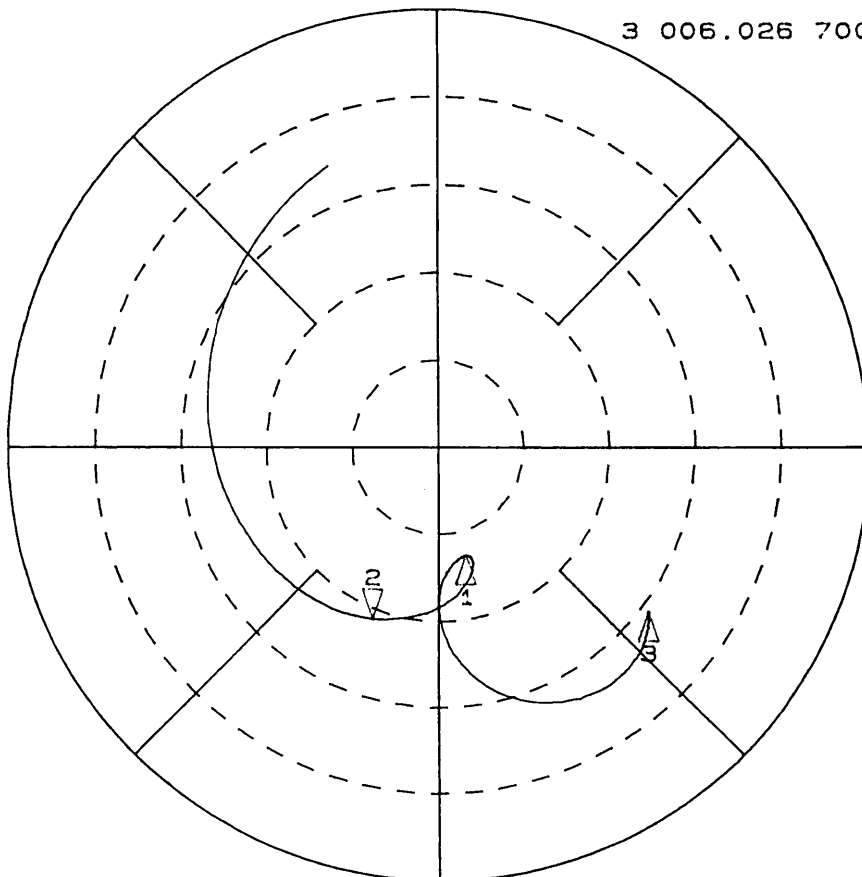
3 006.026 700 MHz

Cor

Avg  
40

Reflection of HCS1

at Output Coupler  
used as input port



1: 3005.620 MHz  
S<sub>11</sub> = -11.8 dB

2: 3006.027 MHz

3: 3005.500 MHz

T = 25.8 °C

x2

CENTER 3 005.500 000 MHz

SPAN

2.000 000 MHz

22.8.97

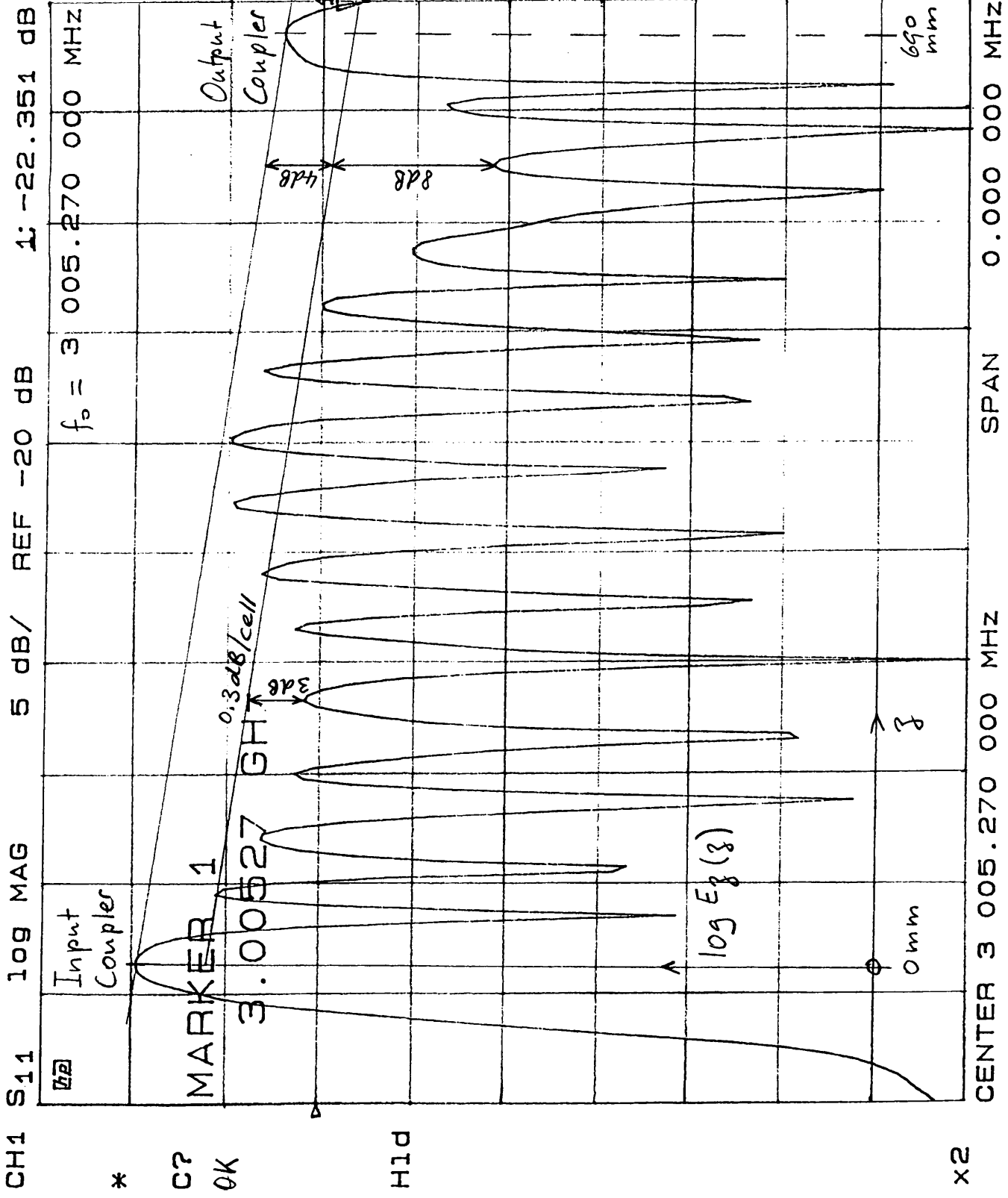


Figure 7

Field Perturbation

by bead  $\phi 1 \times 13 \text{ mm}$

Field Intensity  $\{CS1\}$   
 $S_{11} = 20 \log(E_2/E_0)^2$

1. TWS attenuation is 0.3 dB/cell.
2. Coupler fields are 2 dB higher than cells  
 $E_c = 1.26 E_{avg}$
3. Cell fields vary  $\pm 1.5 \text{ dB}$   
 $E_i = (1 \pm 0.2) E_{avg}$
4. Last cells and output coupler are not matched:  $r \approx 0.5$ .
5. Frequency Correction:  
 $\Delta f = -1080 \text{ kHz}$  for nylon wire - 175 kHz,  
 $T = 27.5^\circ \text{C}$ ,  $\beta = 68\%$ .

Figure 8

HCS1 Phase SM due to Field Perturbation by bead  $\phi$  1x13mm.

$\phi$ : phase measured SM  
 $\psi$ : beam phase advance per cell

$$\psi = \pi - \phi/2$$

$$\langle \psi \rangle = 159^\circ/\text{cell}$$

Frequency Correction

$\Delta f = -1080 \text{ kHz}$  for nylon wire - 175 kHz,  $T = 27.5^\circ \text{C}$ ,  $\mu = 68\%$

